ELSEVIER

Polymer 40 (1999) 2547–2553

polymer

Non-uniform composition profiles in thin film polymeric nanofoams

J.S. Fodor[a], R.M. Briber[a,*], T.P. Russell[b], K.R. Carter[b], J.L. Hedrick[b], R.D. Miller[b], A. Wong[c]

[a]*Materials and Nuclear Engineering Department, 2100 Marie Mount Hall, University of Maryland, College Park, MD 20742, USA*
[b]*IBM Research Division, Almaden Research Center, 650 Harry Rd, San Jose, CA 95120, USA*
[c]*Intense Pulsed Neutron Source, Argonne National Laboratory, 9700 South Cass Ave, Argonne, IL 60439, USA*

Received 9 May 1997; revised 18 June 1998; accepted 21 June 1998

Abstract

Neutron reflectivity (NR) and dynamic secondary ion mass spectroscopy (DSIMS) were used to study compositional variations as a function of film depth in thin polymeric nanofoam films formed from triblock copolymers containing 15 wt%, 13 kg/mol polypropylene oxide end blocks with a fluorinated polyimide center block. The triblock copolymer films were spun cast and imidized on silicon substrates and showed an excess amount of polyimide present at both the air/film and film/substrate interfaces. Upon foaming the films showed a slight densification, and the formation of a 50–150 Å thick polyimide skin at the air interface. The final nanofoam materials had a calculated porosity of roughly 20 vol.% in the center portion of the film.

Keywords: Non-uniform composition profiles; Thin films; Polymeric nanofoams

1. Introduction

Polyimide-based nanofoams are expected to have a significant impact in many technological areas, such as microelectronics, aerospace and membrane science. In recent years the use of polyimides in these areas has steadily increased, due mainly to their relative ease of processing, low dielectric constant, and high thermal and mechanical integrity [1–4]. By incorporating nanoscale voids into polyimide matrices, further reduction of the dielectric constant, density and thermal diffusivity of the bulk material is accomplished, and either closed or open cell porosity may be introduced depending on the morphology and structure of the voids. Past studies [5–18] have indicated that the favorable properties of the polyimide are preserved to a large extent in the polyimide-based nanofoam.

Nanofoams are produced in a three-step process. A triblock copolymer composed of a poly-amic-ester (PAE) center block and two degradable, polypropylene oxide (PO) end blocks are spun cast onto a substrate to form a uniform thin film. The film is then thermally imidized in a reducing atmosphere (Argon) at which time the PAE center block is converted into a polyimide (PI). At this point a microphase-separated morphology exists which is composed of PI and PO microdomains. Subsequent thermal treatment in an oxidizing environment (air) causes the PO domains to decompose into low molecular weight components which can diffuse out of the PI matrix, leaving behind nanoscale voids.

In previous studies [5–18] a variety of polyimides have been considered as the stable matrix block, while polymers such as polymethylmethacrylate (PMMA), polystyrene (PS), poly(α-methylstyrene) (P(α-MS)) and polypropylene oxide (PO) have been considered as the labile blocks. These studies have indicated that stable nanofoams could be produced as shown by thermal gravimetric analysis (TGA) [7,8,12,15,18], density [5–8,12,18], dielectric [7,8] and infrared spectroscopy measurements [9] as well as by small angle X-ray scattering (SAXS) [7,8,18] and transmission electron microscopy (TEM) [5–9,12–14,17,18]. Furthermore, dynamic mechnanical analysis has shown that these materials are structurally stable to 380°C [5,6,8,11–14,18].

Suitability for use in high technology applications requires not only that the foams retain mechanical stability, but also that they have a morphology commensurate with their proposed use. For example, use of the nanofoam in microelectronics as an interlayer dielectric would require solvent resistivity across the film plane and control of the pore size to length scales smaller than that of any features (e.g. lines of metallization) placed on top of them, while use as membranes would require interconnected pores traversing the entire depth of the film. Such morphological features will be dictated by the architecture of the

* Corresponding author. Tel.: +1-301-405-6659; Fax: +1-301-314-9601.

0032-3861/99/$ - see front matter
PII: S0032-3861(98)00487-X

copolymers, as well as by processing conditions. This is especially true when considering the density or compositional variations perpendicular to the film plane.

Both imidization and foaming involve the generation of low molecular weight by-products which diffuse out of the film. Depending upon the relative reaction–diffusion rates, a substantial gradient in by-product composition may exist perpendicular to the film plane. Consequently, the kinetics of the reactions and molecular mobility in the film (due to plastisization effects) may vary with film depth and effect the morphology of the final nanofoam. Furthermore, during imidization, the relatively flexible PAE center blocks are converted into rigid PI chains [19–22]. In polyimide homopolymers (e.g. PMDA–ODA) it has been found that the less flexible PI molecules tend to align parallel to the film surface and are more ordered near the free surface [20–22]. Similar behavior may be expected to occur in our system; however, the organization of the molecules will also be governed by the thermodynamics of the microphase separation. Finally, energetic interactions at the air/film and film/substrate interfaces can also lead to compositional and density variations with film depth.

Neutron reflectivity (NR) and dynamic secondary ion mass spectroscopy (DSIMS) are used to investigate the imidized (unfoamed) copolymer film and the effects of foaming on composition as a function of depth of the sample. Studies were performed on ~1000 Å thick films of the imidized copolymer during the foaming process. The data indicate that the density of the film is not uniform as a function of depth in that there is an excess of polyimide at both the air/film and the film/substrate interfaces in the imidized film, and a slight densification of the film occurs during foaming. These results are explained by an increase of order in the polyimide center blocks near the interfaces or by a partial collapse of the foam at these interfaces.

2. Experimental

2.1. Materials and sample preparation

Studies were conducted on a triblock copolymer composed of a 3F/PMDA (3F-diamine/pyromelletic dianhydride) poly-amic-ester center block and two polypropylene oxide end blocks. Synthesis of the individual blocks and the triblock, as well as its chemical structure are described elsewhere [9]. The PO end blocks had a molecular weight of 13 kg/mol, and the total PO content was 15 wt% as determined by NMR. Based on the PO content the calculated 3F/PMDA molecular weight was 147 kg/mole. Silicon wafers were cleaned by immersing them in a sulfuric acid solution containing a few percent hydrogen peroxide at 120°C for 1 h. Upon removal from the solution they were rinsed thoroughly with de-ionized water and dried with ultra-pure nitrogen. The wafers were then treated with a buffered oxide etch, again rinsed thoroughly with de-ionized water, blown dry with ultra-pure nitrogen, and set on a hot plate at 150°C for ~1/2 h to remove any absorbed water. For all experiments the PO–(poly-amic-ester)–PO triblock was dissolved in cyclohexanone and spun cast onto silicon wafers. Samples for neutron reflectivity were prepared on 5.08 cm diameter × 4.76 mm thick wafers, while DSIMS and XPS samples were prepared on 2.54 cm diameter × 0.3 mm thick wafers. After spinning, the samples were placed under an argon (oxygen free) atmosphere and heated at 5°C/min to 250°C, held there for 1 h, ramped again at 5°C/min to 300°C, held at that temperature for 1 h, and then allowed to cool to room temperature. The DSIMS samples were then split into two pieces. Half of each sample was foamed by heating under air at 5°C/min to 300°C and holding for 4 h. The neutron reflectivity data was collected at room temperature with the samples being foamed between reflectivity measurements, enabling comparisons to be made on the same films throughout the foaming process.

2.2. Dynamic secondary ion mass spectroscopy

DSIMS measurements were obtained using a Perkin Elmer 6300 secondary ion mass spectrometer. The primary ion beam species was O_2^+ supplied at an energy of 2 keV (200 nA directed 60° from the surface normal). The ion beam was rastered to create a crater of 500 × 500 μm^2. Secondary ions were collected from the central 9% of the sputtered crater. The number of secondary ions detected in the mass spectrometer was determined as a function of time. The time scale was then converted to a depth scale using the appropriate factor. Since fluorine is contained only in the polyimide, monitoring the relative amount of fluorine as a function of depth yields information concerning the relative amount of polyimide as a function of film depth. The resolution of the technique is about ~50 Å.

2.3. Neutron reflectivity

Neutron reflectivity (NR) experiments were conducted on the instrument POSY2 at the Intense Pulsed Neutron Source (IPNS) at Argonne National Laboratory [23] which makes use of a spallation neutron source. The experimental set-up has been described thoroughly in the literature [23]. With this technique a high degree of resolution can be obtained. Thorough explanations of the technique can be found elsewhere [24–26]. Briefly, for a spallation source, a well collimated neutron beam of known wavelength distribution impinges on the sample at a grazing angle, θ, and the beam's reflected intensity is detected. Through a time-of-flight (TOF) analysis the reflectivity, R, can be determined as a function of the neutron momentum (impinging on the sample) perpendicular to the film plane, $k_{0,z}$, where

$$k_{0,z} = \frac{2\pi}{\lambda}\sin\theta \quad (1)$$

The refractive index for neutrons, μ_j, in a medium having a

scattering length density, b/V_j, is given by, $\mu_j = [1 - \lambda^2(b/V_j)/2\pi]^{1/2}$. Therefore, the neutron momentum, $k_{j,z}$ in medium j is given by

$$k_{j,z} = [k_{0,z}^2 - 4\pi(b/V_j)]^{1/2} \quad (2)$$

For values of $k_{0,z}$ below a critical value determined by the scattering length density of the film, $k_{cr} = 2\pi(b/V)^{1/2}$, the neutrons are totally externally reflected ($R = 1$). For a single film of non-varying scattering length density on a substrate with perfectly smooth interfaces standard optical methods [24–27] give as the reflectivity

$$R = \left| \frac{r_{01} + r_{12}e^{2i\beta}}{1 + r_{01}r_{12}e^{2i\beta}} \right|^2 \quad (3)$$

where

$$r_{ij} = \frac{k_i - k_j}{k_i + k_j} \quad (4)$$

$\beta = k_1 d_1$, where d_1 is the film thickness, and the indices 0, 1 and 2 stand for the air, film and substrate, respectively.

For films having a non-uniform scattering length density as a function of film depth, the film is divided into N layers each having a uniform scattering length density. Reflection can then be modeled as taking place at each layer boundary. Eq. (3) was derived by conservation of momentum and continuity of the neutrons at the air/film and film/substrate interfaces. An expression for the reflectivity of the multilayered system is obtained following a similar strategy, however, $N + 1$ interfaces exist. Here matrix methods have been derived [25,28,29] to obtain an expression for the reflectivity.

$$R = \frac{M_{21}M_{21}^*}{M_{11}M_{11}^*} \quad (5)$$

where the matrix, $\mathbf{M}$, is defined by $\mathbf{M} = \mathbf{M}_1\mathbf{M}_2\mathbf{M}_3\cdots\mathbf{M}_N$, and each $\mathbf{M}_j$ is a characteristic matrix containing information on the jth interface

$$M_j = \begin{bmatrix} e^{i\beta_{j-1}} & r_j e^{i\beta_j} \\ r_j e^{-i\beta_{j-1}} & e^{-i\beta_{j-1}} \end{bmatrix} \quad (6)$$

with

$$r_j = \frac{k_{j-1} - k_j}{k_{j-1} + k_j} \quad (7)$$

and $\beta_j = k_j d_j$.

The above derivation assumes perfectly smooth interfaces, while in reality each surface may contain a certain degree of roughness. Interfacial roughness can be incorporated into the model by assuming a Gaussian distributed height–height correlation function at the interface [30], with a root mean squared height distribution, $\langle\sigma\rangle$. Roughness can then be introduced at each interface by re-defining the reflection, r_j, in Eq. (8) (with $q_j = 2k_j$) [24,25,30]

$$r_j = \frac{k_{j-1} - k_j}{k_{j-1} + k_j} e^{[-0.5(q_{j-1}q_j\langle\sigma\rangle^2)]} \quad (8)$$

The scattering length density profile of non-uniform films can be obtained using Eqs. (5)–(8) by finding the profile that minimizes the discrepancy between the calculated and experimental reflectivity.

3. Results and discussion

NR was used to follow compositional changes in an initially 910 Å thick film at various stages during foaming. Fig. 1 shows data collected on an imidized copolymer prior to foaming and after 1, 2 and 4 h foaming time. Foaming between data aquisition was accomplished by heating samples to 300°C at 5°C/min, holding for the set time then cooling to room temerature. This procedure was repeated until complete foaming (4 h total time at 300°C) was accomplished. The mode of aquisition did require several heating and cooling cycles, however, by acquiring data on the same sample during foaming rather than using several samples foamed to various levels of completion, experimental variations in film thickness, spinning conditions and thermal history were eliminated.

In Fig. 1, the local minima in the reflectivity curves result from destructive interference brought about from the path length difference between neutrons reflected from the air/film and film/substrate interfaces. They are related to the film thickness by $t_{film} = \pi/\Delta k_{0,z}$, where $\Delta k_{0,z}$ is the spacing between minima. The spacing, $\Delta k_{0,z}$, increases with

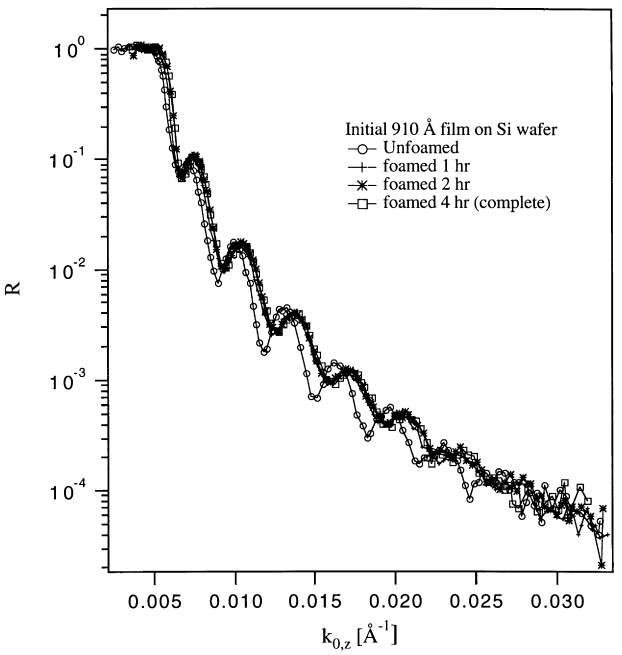

Fig. 1. Neutron reflectivity data for an initially 910 Å thick film prior to and at various stages during foaming.

increased foaming time, indicating a moderate thinning of the film. This is accompanied by a shift in the critical edge, k_{cr} to larger $k_{0,z}$, indicating an overall increase in the average scattering length density of the film. Both events, film thinning and densification, are characteristic of a slight collapse of the nanofoam. Additionally, for a perfectly smooth interface the reflectivity at large $k_{0,z}$, R_s, decays in magnitude as $k_{0,z}^4$, $R_s \propto k_{0,z}^{-4}$. Roughness at the air/film interface, however, results in a steeper decrease in reflected intensity, $R_r = R_s \exp(-4k_{0,z}k_{1,z}\langle\sigma\rangle^2)$, where R_r is the reflectivity for a rough surface, $k_{0,z}$ and $k_{1,z}$, are described previously and $\langle\sigma\rangle$ is the root mean squared surface roughness. As evident in Fig. 1, the intensity of the reflectivity at high $k_{0,z}$ is fairly constant during the foaming process which indicates that there is not a substantial change in surface roughness. Calculated reflectivity curves, as discussed below, required 15 Å surface roughness in the unfoamed material to effectively model the data. This value did not change during foaming, indicating that large-scale surface imperfections were definitely not present in the copolymer film nor did they arise during the foaming process. Such a result is very encouraging in light of the requirements for microelectronics application. Large-scale anomalies at the surface could hamper the use of nanofoams as packaging materials. It should be noted that the present result does not rule out the possibility of a thin PO layer at the film surface. Since the scattering length density of PO (0.34×10^{-6} Å^{-2}) is close to that of air (0.0 Å^{-2}), a thin PO layer at the surface would appear as a surface roughness.

Figs 2 and 3 show the reflectivity curves corresponding to the unfoamed copolymer and the completely foamed film along with model fits of the data calculated from Eqs. (5)–(8). The scattering length density profiles used to calculate the models are shown in the insets. Air/film and film/substrate interfacial roughness of 15 and 8 Å, respectively,

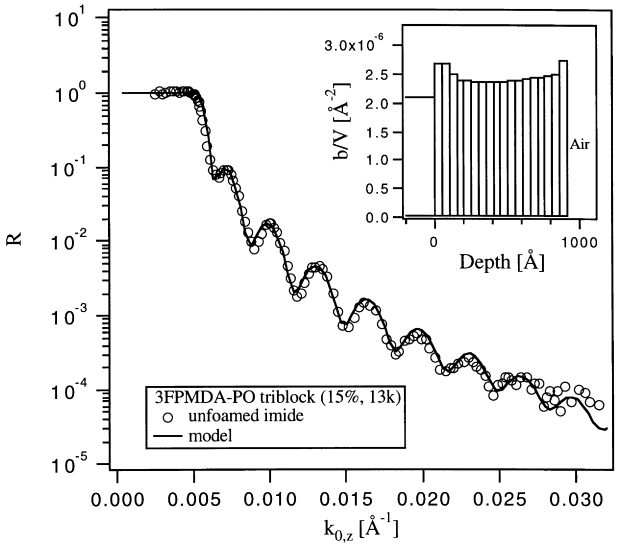

Fig. 2. Neutron reflectivity data for a 910 Å thick copolymer film (imidized, unfoamed) plotted along with a model fit of the data. The scattering length density profile used to obtain the model is shown in the inset.

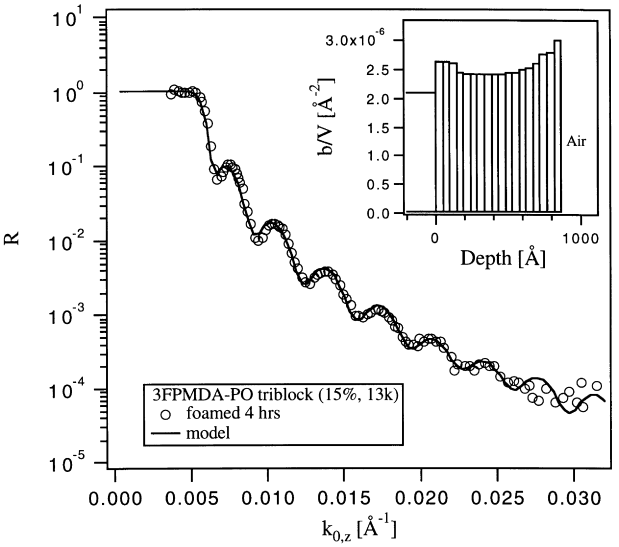

Fig. 3. Neutron reflectivity data for the film shown in Fig. 2 after 4 h foaming time at 300°C. Plotted along with the data is a model fit using the scattering length density profile shown in the inset.

were used to model the unfoamed copolymer data, while 15 and 9 Å were used in modelling the foamed film. Modeling of the data taken during the intermediate foaming steps was not performed since only very slight changes are evident in the data after 1 h of foaming (see Fig. 1). Since the scattering length density of the 3F/PMDA polyimide (3.13×10^{-6} Å^{-2}) is significantly different from that of PO and that of a void, the average composition of each slab will be evident from the magnitude of the scattering length density of that slab, the closer the value is to 3.13×10^{-6} A^{-2} the higher the content of polyimide in that slab. Consequently, the scattering length density profiles indicate that in both the unfoamed and foamed films there is clearly an increased amount of polyimide at the interface. This is discussed further below.

The scattering length density profiles of the unfoamed and foamed film are compared in Fig. 4. Two important features are immediately evident: (1) the scattering length density profile, and thus, the composition vary with film depth both prior to and subsequent to foaming; and (2) the film thickness decreases by roughly 5% during the foaming process. The higher scattering length density near the air/film and film/substrate interfaces prior to foaming indicates that these regions contain a higher concentration of polyimide (or less/smaller PO domains) relative to the center of the film. Recalling that the initial PAE–PO triblock contained 15 wt% PO, accounting for mass loss during imidization (loss of C_2H_5OH), and using as the density of the polyimide and PO phase, $\rho_{PI} = 1.35$ g/cm^3 [13], and $\rho_{PO} = 1.0$ g/cm^3 [31], respectively, the imidized copolymer film should contain 21.4 vol.% PO. At the air interface $b/V \sim 2.75 \times 10^{-6}$ Å^{-2}, suggesting a local composition (based on the b/V values for pure PO and 3F-PI) of ~13 vol.% PO. Near the film/substrate interface the PO content is calculated to be ~16 vol.% while in the center portion of the

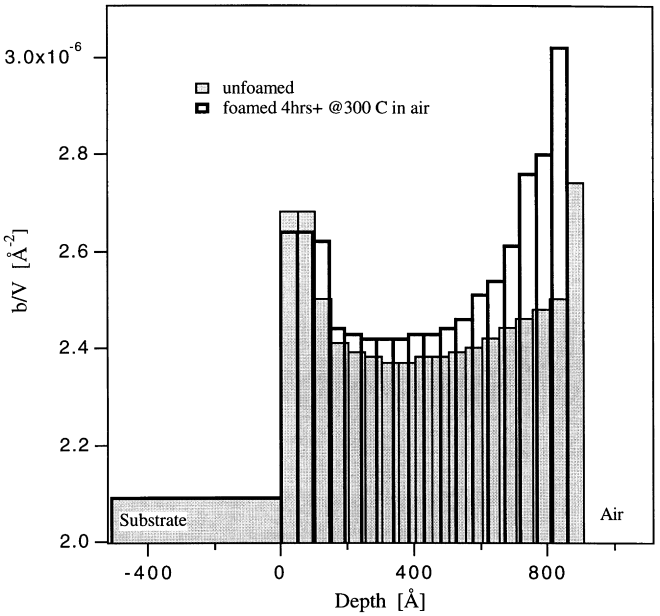

Fig. 4. Comparison of the scattering length density profiles for the unfoamed and foamed samples.

film it is ~23 vol.%. The fact that the center portion of the film has a composition of PO greater than that calculated for the bulk material might indicate that there is a small amount of homopolymer contained in the triblock, and that it is non-uniformly distributed in the thin film. However, the modeled reflectivity profile was less sensitive to changes in the magnitude of the scattering length density in the center portion of the film. Therefore, a 1.6 vol.% difference in PO content between the bulk value and that in the center portion of the film is within the experimental uncertainty.

After foaming, the scattering length density near the air/film interface increases becoming comparable to that of the pure polyimide, indicating the formation of a thin (50–150 Å) polyimide skin at the air/film interface, while only slight changes are observed at the film/substrate interface. At both interfaces there is an increase in the breadth of the dense regions. Also evident, and somewhat counter-intuitive, is the increase in the scattering length density in the center portion of the film upon foaming. (This increase is consistent with the shift in the critical edge, k_{cr}, to larger $k_{0,z}$, as discussed earlier.) If the PO domains are decomposing and being replaced by voids, the average scattering length would be expected to decrease. Upon closer examination, however, this slight increase is consistent with the 5% decrease in film thickness. This decrease is brought about by both the formation of the polyimide skin at the air/film interface and a partial collapse of the foam in the central region of the film. In the final nanofoam the porosity in the center portion of the film is ~22 vol.%.

DSIMS data were obtained on unfoamed and foamed films of a similar thickness (950 Å). Fig. 5(a)–(b) shows the secondary ion counts obtained for fluorine in the DSIMS experiments. In the 3F/PMDA–PO copolymer and nanofoam film, the relative amount of fluorine as a function of depth allows the detection of the relative amount of the polyimide as a function of film depth, since fluorine is contained in the polyimide and not the PO domains or voids. Both the unfoamed and foamed specimens show similar trends. Upon foaming, the depth dependence of the fluorine signal does not change significantly. It is difficult from the data alone to state whether there has been any change in the film thickness. The 5% change indicated by the NR results may not be detectable in these studies since slight variations between experimental runs could mask out this effect, i.e. a 5% (~45 Å) change is below the instrument resolution. However,it is quite evident that there has not been a significant densification of the film and that the structure of the film has remained intact upon foaming. Therefore, the DSIMS results, in agreement with the NR results, show that the foam structure has been retained and only a slight, if any, collapse of the structure has occurred.

The results of the DSIMS and NR experiments are consistent with one another, in that excess of polyimide is seen at both the air and substrate interfaces. The differences in the shapes of the profiles can be attributed to the fact that DSIMS data is following only the fluorine content while the NR experiment provides information on the overall scattering length density profile.

The distance over which an increased scattering length density (NR) and excess in the fluorine signal (DSIMS) is observed extends over a relatively large distance at both the air/film and film/substrate interfaces with a lower local maxima at the film/substrate interface relative to that at the air/film interface. Additionally, there is no marked depression in the scattering length density (indicating an excess of PO) on either side. Thus, this surface excess cannot be attributed to the segregation of the 3F/PMDA block to the interfaces. Both the size scale and the shape of the concentration

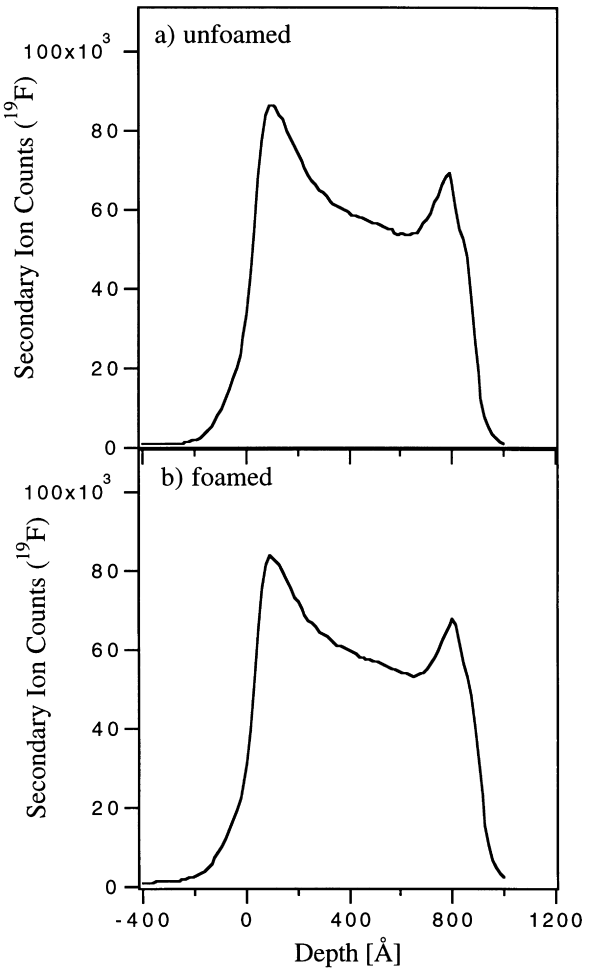

Fig. 5. DSIMS data showing the secondary ion count of fluorine in a 950 Å thick film of (a) an imidized, unfoamed copolymer; (b) a sample foamed for 4 h at 300°C.

profile, i.e. monotonically decreasing, are inconsistent with the segregation of a block to an interface. The only possible source of these interfacial excesses is the presence of 3F/PMDA homopolymer originating from unreacted center block during the synthesis of the triblock copolymer. Only a small fraction of unreacted homopolymer could, provided the homopolymer preferentially segregated to the surface, give rise to a substantial excess at the interfaces. Unfortunately, no solvent was found to perform the homopolymer extraction quantitively. The enhanced concentration of 3F/PMDA at the interfaces would also give rise to smaller PO microdomain sizes which are more prone to collapsing during the foaming process.

Both the neutron and DSIMS studies, therefore, indicate that the concentration of 3F/PMDA is not uniform as a function of depth and that effectively a skin of the 3F/PMDA has formed at the interfaces. For membrane applications such a skin would be deleterious, since it would retard the diffusion of material through the membrane. However, for applications in microelectronics where such materials would be used in multilayered structures, this homopolymer skin might be quite attractive. Since the voids present in the nanofoam are interconnected [17], this polyimide skin would impede the penetration of solvent and/or water into the foam structure, thereby, reducing the inclusion of very mobile impurities in the foam which would hamper the performance of the device.

Results from TEM studies on films made from these same polymers have been recently published [17] and these studies indicate that the foaming process results in clearly defined interconnected voids in the film. This result is also supported by small-angle neutron scattering studies on similar films. Even with the void structure as observed by TEM, there did not appear to be a problem with loss of specular reflectivity due to off-specular scattering as the reflectivity fringes continue out to reasonably high k values ($k > 0.03$ Å^{-1}).

4. Conclusions

Neutron reflectivity and dynamic secondary ion mass spectroscopy studies on thin (910 Å) films indicate excess polyimide content at the air and substrate interfaces. Upon foaming, the film shrinks in thickness by about 5% due to further decreases in porosity at the air/film interface and a very slight constriction of the pores in the center portion of the film. In the final nanofoam film the interfacial skin was determined to be pure polyimide, while the center portion of the film had a calculated porosity of about 22 vol.%. The development of the interfacial skin is likely brought on by 3F/PMDA homopolymer present in the triblock copolymer which preferentially segregates to the interfaces.

Acknowledgements

The authors would like to acknowledge the support of the Advanced Technology Program of NIST under cooperative agreement 70NANB3H1365 and of IBM. Additionally, this work has benefited from the use of the Intense Pulsed Neutron Source at Argonne National Laboratory, funded by the US Department of Energy, BES-Materials Science, under Contract W-31-109-Eng-38.

References

[1] Wilson D, Stenzenberger HD, Hergenrother PM, editors. Polyimides. Oxford: Blackie and Sons, 1990.
[2] Tummala RR, Rymaszewski EJ. Microelectronics packaging handbook. New York: Van Nostrand Reinhold, 1989.
[3] Lupinski JH, Moore RS, editors. Polymeric materials for electronics packaging and interconnection. ACS Symposium Series 407, 196th National Meeting of the American Chemical Society, Los Angeles, CA, 1988. Washington, DC: ACS Publishing, 1989.
[4] Hiroshi I, Seiichi T, Kazuyuki H, editors. Polymeric materials for microelectronic applications. ACS Symposium Series 579, Polymers

for Microelectronics 1993 Meeting, Kawasaki, Japan, 1993. Washington, DC: ACS Publishing, 1994.
[5] Carter KR, Labadie JW, DiPietro RA, Sanchez MI, Russell TP, Swanson SA, Auman BC, Lakshmanan P, McGrath JE. Polymer Preprints (Am Chem Soc, Div Polym Mater Sci Eng) 1995;72:383.
[6] Charlier Y, Hedrick JL, Russell TP, DiPietro R. Polymer Preprints (Am Chem Soc, Div Polym Mater Sci Eng) 1995;72:389.
[7] Labadie JW, Hedrick JL, Wakharkar V, Hofer DC, Russell TP. IEEE Trans Compon Hybrids Manuf Technol 1992;15:925.
[8] Hedrick JL, Labadie JW, Russell TP, Hofer DC, Wakharkar V. Polymer 1993;34:4717.
[9] Sanchez MI, Hedrick JL, Russell TP. J Polym Sci Polym Phys Ed 1995;33:253.
[10] Charlier Y, Hedrick JL, Russell TP. Polymer 1995;36:4529.
[11] Charlier Y, Hedrick JL, Russell TP, Swanson S, Sanchez M, Jéróme R. Polymer 1995;36:1315.
[12] Charlier Y, Hedrick JL, Russell TP, Jonas A, Volksen W. Polymer 1995;36:987.
[13] Hedrick JL, Hawker CJ, DiPietro R, Jéróme R, Charlier Y. Polymer 1995;36:4855.
[14] Hedrick JL, DiPietro R, Charlier Y, Jéróme R. High Perform Polym 1995;7:133.
[15] Miller RD, Carter KR, Cha H-J, DiPietro RA, Hawker CJ, Hsu B-L, Labadie JW, Russell TP. Polymer Preprints (Am Chem Soc, Div Polym Chem) 1996;37 (1):148.
[16] McGrath JE, Jayaraman SK, Lakshmanan P, Abed JC, Afchar-Taromi F. Polymer Preprints (Am Chem Soc, Div Polym Chem) 1996;37 (1):136.
[17] Fodor JS, Briber RM, Russell TP, Carter KR, Hedrick JL, Miller RD. J Polym Sci: Polym Phys Edn 1997;35:1067.
[18] Carter KR, Cha HJ, DiPietro RA, Hawker CJ, Hedrick JL, Labadie JW, McGrath JE, Russell TP, Sanchez MI, Swanson SA, Volksen W, Yoon DY. Mater Res Soc Symp Proc 1995;381:79.
[19] Odian G. Principles of polymerization. New York: McGraw-Hill, 1970.
[20] Saraf RF, Dimitrakopoulos C, Toney MF, Kowalczyk SP. To appear in Langmuir, 1996.
[21] Poon TW, Saraf RF, Silverman BD. Macromolecules 1993;26:3369.
[22] Factor BJ, Russell TP, Toney MF. Macromolecules 1993;26:2847.
[23] Karim A, Arendt BH, Goyette R, Huang YY, Kleb R, Felcher GP. Physica B 1991;173:17.
[24] Anastasiadis SH, Russell TP, Satija S, Majkrzak CF. J Chem Phys 1990;92:5677.
[25] Penfold J, Thomas RK. J Phys: Condens Matter 1990;2:1369.
[26] Higgins JS, Benoît HC. Polymers and neutron scattering. Oxford: Claredon Press, 1994.
[27] Russell TP. Mater Sci Rep 1990;5:171.
[28] Heavens OS. Optical properties of thin films. London: Butterworth, 1955.
[29] Lekner J. Theory of reflection. Boston, MA: Martinus Nijhoff, 1987.
[30] Cowley TL, Ryan TW. J Phys D: Appl Phys 1987;20:61.
[31] Brandrup J, Immergut EH, editors. Polymer handbook, 2nd ed. New York: Wiley, 1975.